Responses of East Asian summer monsoon to historical SST and atmospheric forcing during 1950–2000

Hongmei Li · Aiguo Dai · Tianjun Zhou · Jian Lu

Abstract The East Asian summer monsoon (EASM) circulation and summer rainfall over East China have experienced large decadal changes during the latter half of the 20th century. To investigate the potential causes behind these changes, a series of simulations using the national center for atmospheric research (NCAR) community atmospheric model version 3 (CAM3) and the geophysical fluid dynamics laboratory (GFDL) atmospheric model version 2.1 (AM2.1) are analyzed. These simulations are forced separately with different historical forcing, namely tropical sea surface temperature (SSTs), global SSTs, greenhouse gases plus aerosols, and a combination of global SSTs and greenhouse gases plus aerosols. This study focuses on the relative roles of these individual forcings in causing the observed monsoon and rainfall changes over East Asia during 1950–2000. The simulations from both models show that the SST forcing, primarily from the Tropics, is able to induce most of the observed weakening of the EASM circulation, while the greenhouse gas plus (direct) aerosol forcing increases the land-sea thermal contrast and thus enhances the EASM circulation. The results suggest that the recent warming in the Tropics, especially the warming associated with the tropical inter-decadal variability centered over the central and eastern Pacific, is a primary cause for the weakening of the EASM since the late 1970s. However, a realistic simulation of the relatively small-scale rainfall change pattern over East China remains a challenge for the global models.

1 Introduction

Associated with the Pacific (inter)decadal oscillation (PDO) (Deser et al. 2004), atmospheric large-scale circulation experienced a decadal shift in the late 1970s in the Northern Hemisphere (Trenberth and Hurrell 1994). For example, the East Asian summer monsoon (EASM) has weakened since the late 1970s, which is characterized by the weakening of the 850 hPa southwesterly winds, southward shift of the 200 hPa jet stream, and increases in sea level pressure over East Asia (Hu 1997; Wang 2001; Guo et al. 2003; Hu et al. 2003; Wang and Ding 2006; Xu et al. 2006). Furthermore, a cooling trend in the upper troposphere and lower stratosphere over East Asia has led to the weakening in the northward progression of southerly monsoon winds over this region (Yu et al. 2004; Yu and Zhou 2007). The EASM is also influenced by the El Niño-southern oscillation (ENSO) (Wang et al. 2000; Lau and Weng 2001; Wu et al. 2003), with the correlation between the rainfall over East China and the winter Niño–3.4 SST index showing pronounced differences between developing and decaying ENSO years (Wu et al. 2003). The ENSO-EASM relationship has experienced a significant decadal change, with the El Niño-stimulated circulation weakening the EASM after the late 1970s (Wu and Wang 2002).

H. Li · T. Zhou (✉)
LASG, Institute of Atmospheric Physics, Chinese Academy of Sciences, Beijing, China
e-mail: zhoutj@lasg.iap.ac.cn

A. Dai · J. Lu
National Center for Atmospheric Research, Boulder, CO, USA

H. Li
Graduate School of Chinese Academy of Sciences, Beijing, China
e-mail: lihm@mail.iap.ac.cn

Associated with the weakening of the EASM, rainfall over East China also has experienced a significant change since the late 1970s, with the Yangtze River Valley becoming wetter and the Yellow River Valley becoming drier in recent decades, a pattern often referred to as "southern flooding and northern drought" in China (Yatagai and Yasunari 1994; Nitta and Hu 1996; Weng et al. 1999; Xu 2001; Hu et al. 2003; Yu and Zhou 2007; Li et al. 2008). This rainfall change has caused severe droughts in North China and frequent flooding along the Yangtze River during recent decades, causing large losses in human lives and enormous damages to local economies.

Studies on the causes of the EASM weakening and the accompanying rainfall changes have pointed to several factors. Many studies suggest that recent warming in the tropical Pacific and India Ocean leads to an abnormal Subtropical Pacific High that reduces water vapor transport to North China from South China Sea and thus contributes to the observed rainfall changes there (Hu 1997; Chang et al. 2000; Gong and Ho 2002; Hu et al. 2003; Zhou and Huang 2003; Yang and Lau 2004). In particular, Zeng et al. (2007), through analyses of model simulations using the National Center for Atmospheric Research (NCAR) community atmospheric model version 3 (CAM3) forced by observed sea surface temperature (SSTs), suggest that the recent warming in the North Indian Ocean and around the South China Sea may have played an important role in the recent EASM weakening. This mechanism is also supported by the responses of five atmospheric general circulation models (AGCMs) to specified Indian Ocean-Western Pacific warming (Zhou et al. 2008a). The warming in tropical central and eastern Pacific Ocean may also have contributed to the recent decreases in global land monsoon rainfall (Wang and Ding 2006; Zhou et al. 2008b, c). Other studies, however, have linked the EASM weakening to the PDO in the North Pacific (Yang et al. 2005; Ma and Fu 2007). The oceanic forcing from the Tropics and the North Pacific may be intrinsically linked, as recent studies (Deser et al. 2004; Deser and Phillips 2006) show that the Tropics play a key role in North Pacific interdecadal climate variability.

There are also studies linking the rainfall changes to increased aerosols from air pollution over East Asia. The aerosols can affect local convective motion through their direct and indirect reduction of short-wave solar radiation, and they can also affect cloudiness and the auto-conversion from cloud water into rainwater by changing cloud condensation nuclei (Xu 2001; Menon et al. 2002; Qian et al. 2003; Huang et al. 2006), and the aerosol indirect effects may dominant over that of direct effects (Qian and Giorgi 1999). Furthermore, decadal variations associated the North Atlantic Oscillation is also linked to recent climate changes over East Asia through atmospheric teleconnection (Yu and Zhou 2004; Li et al. 2005; Xin et al.

2006). It is possible that all these factors may have played some roles in recent climate changes over East Asia; however, their relative contributions are unclear in explaining the observed EASM weakening and rainfall changes.

The purpose of our study is to investigate the effects of observed changes in SSTs, greenhouse gases, and aerosols during 1950–2000 on East Asian climate, especially their relative contributions to the observed monsoon circulation and rainfall changes. We make use of surface observations, atmospheric reanalyses, and more importantly, a series of ensemble simulations using NCAR CAM3 and geophysical fluid dynamics laboratory (GFDL) atmospheric model version 2.1 (AM2.1) forced by various historical forcings. By using two models, we are able to compare and isolate robust responses to a given forcing. In this paper, we mainly focus on the effects of observed changes in SSTs and greenhouse gases.

The rest of the paper is organized as follows. In Sect. 2, we describe the data, models and simulations used in this study. The results are presented in Sect. 3, and a summary is given in Sect. 4.

2 Data, models and simulations

The NCEP/NCAR (Kalnay et al. 1996) and ERA-40 (Uppala et al. 2005) reanalysis data of atmospheric circulation were used for comparison with model simulations. Here we used the precipitation data from Chen et al. (2002) (although we also examined other precipitation data sets), and PDO index data from Zhang et al. (1997). The two models used in this study are the NCAR CAM3 (Collins et al. 2006) and GFDL AM2.1 (GFDL Global Atmospheric Model Development Team 2004). The CAM3 version used here employs an Eulerian dynamic core on a T85 ($\sim$1.4°) grid and 26 vertical levels. The AM2.1 uses a finite-volume dynamical core on a 2° lat × 2.5° lon grid with 24 vertical levels.

Four sets of ensemble runs under different forcings from 1950 to 2000 were performed with CAM3 and AM2.1, detailed information on the ensemble runs is listed in Table 1. The GOGAI runs (all forcing runs) were forced by observed global SSTs plus historical evolution of atmospheric forcing (observed greenhouse gases, aerosols, tropospheric and stratospheric ozone, and solar irradiance) as used in the Intergovernmental Panel on Climate Change (IPCC) 20th century runs (Dai et al. 2001). The SST dataset was a blended version of the HadISST and Reynolds dataset (Hurrell et al. 2008). Only the direct radiative effect of aerosols was considered in these model runs. The indirect effects of aerosols will be considered as the newer versions of the models that include such parameterizations become available. The GOGA (referred to as global ocean global atmosphere) runs were forced by

Table 1 Number of ensemble runs from 1950 to 2000 under different forcing scenarios used in this study

Model\forcing	GOGA	TOGA	GOGAI	RADATM
NCAR CAM3 (T42)	5	5	5	10
NCAR CAM3 (T85)	5	5	5	N/A
GFDL AM2.1	10	N/A	10	N/A

GOGA global SST forcing, i.e., the AGCM is forced by observed monthly SSTs over the global oceans from 1950 to 2000, *TOGA* Same as GOGA but forced only by tropical (20°S-20°N) SSTs with extra-tropical SSTs fixed to climatological monthly SSTs, *GOGAI* global SST plus IPCC 20th century atmospheric (primarily greenhouse gases and direct aerosol) forcings, and *RADATM* climatological monthly SST plus the IPCC 20th century atmospheric forcings

the historical global SSTs with fixed atmospheric forcings (set to the 1990 level). The TOGA (referred to as tropical ocean global atmosphere) runs were forced by the time-varying tropical (20°S–20°N) SSTs and fixed climatological SSTs (with seasonal cycle) polewards of 30° lat, with linear interpolation between 20° and 30° lat. The atmospheric forcings were fixed at the 1990 level in the TOGA runs. The RADATM (referred to as atmospheric forcing) runs were forced by climatological monthly SSTs and the IPCC time-varying atmospheric forcings during 1950–2000. The RADATM runs were only available for the CAM3 at T42 resolution ($\sim 2.8°$).

After comparing several commonly used EASM indices (e.g., Guo et al. 2003; Zeng et al. 2007), we adopted the index proposed by Han and Wang (2007) who followed Webster and Yang (1992) but applied to the East Asian domain. It is defined as the normalized zonal wind (u) shear (or difference) between 850 and 200 hPa averaged over 20°–40°N and 110°–140°E. This zonal wind shear-based EASM index (EASMI) is closely linked to the convective activity over the western Pacific, and provides a first-order approximation of the strength of the strongest baroclinic mode that has the dominant effect on the EASM (Wang et al. 1999). Following Xu (2001) and Li et al. (2008), we also defined a precipitation difference index (PDI) as the difference of normalized precipitation between North China (33°–41°N, 105°–122°E) and the Yangtze River Valley (27°–32°N, 105°–122°E). According to Deser and Phillips (2006), we chose 1976/1977 as the climate transition years. We focused on the composite difference between 1977 and 2000 and 1950–1976 (1958–1976 for ERA-40 data), although time series and correlations were also examined for some of the variables. We should notice that even if the correlation coefficients are not statistically significant because of models' deficiency in producing high frequency variability, it does not disapprove models' ability in simulating low frequency variability, such as long term trends and decadal changes. The Student *t* test is used to evaluate the significance of the composite difference.

We found that the composite differences are comparable among the individual ensemble runs, thus we only show the ensemble-mean results in this paper.
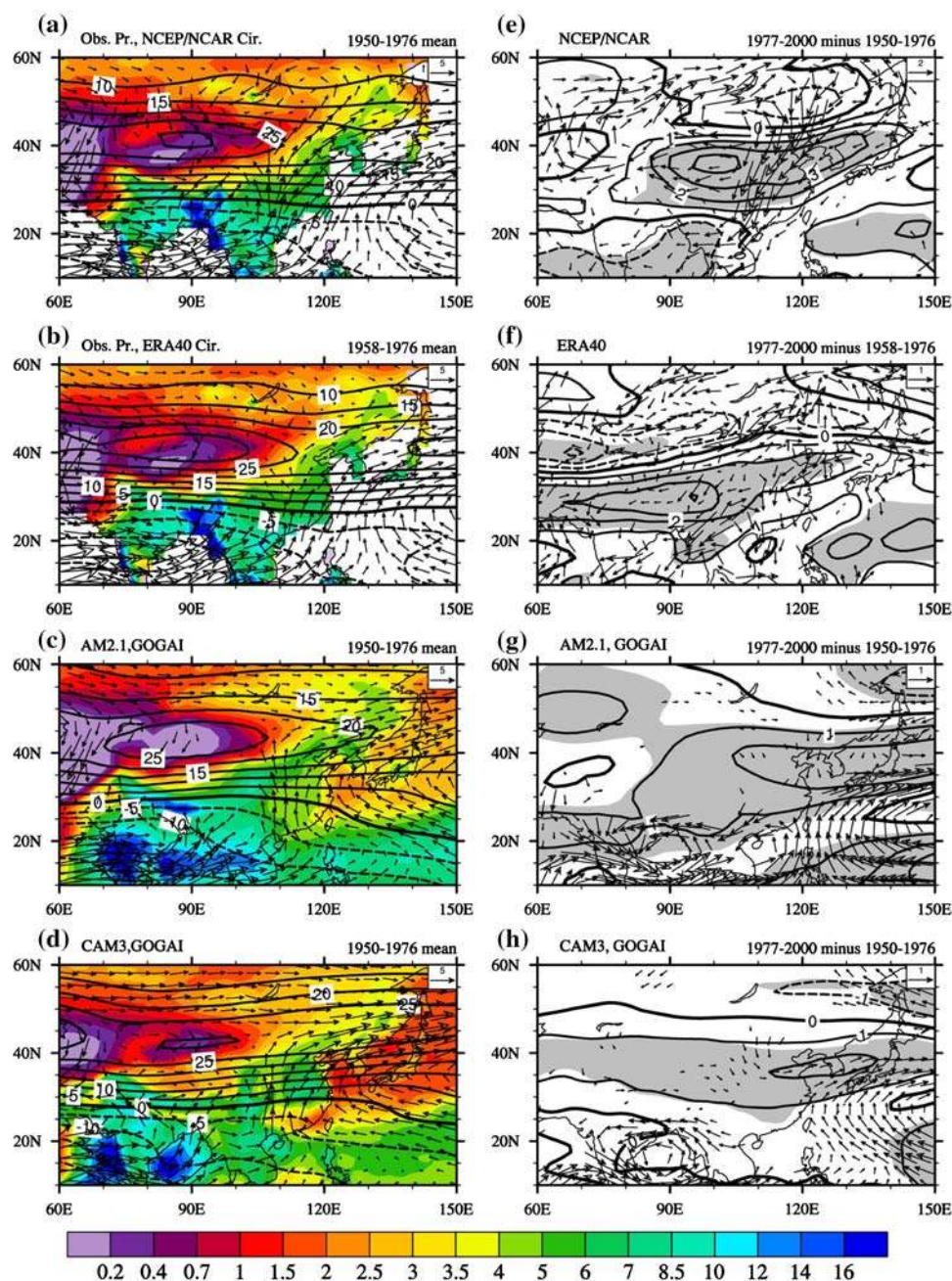
3 Results

3.1 EASM's response to all forcings

The combination of SST and IPCC atmospheric forcings, as in the GOGAI runs, represents the most realistic forcing scenario, and thus the most likely case for the models to reproduce the observed changes.

Variations in the EASM are usually described using summer rainfall, low level (850 hPa) winds, and 200 hPa jet stream (e.g., Zhou and Yu 2005; Zhang et al. 2006; Yu and Zhou 2007). Figure 1a, b shows the 1950–1976 composite mean of June–August (JJA) precipitation from observations and 850 hPa vector winds and 200 hPa zonal wind from the NCEP/NCAR and ERA-40 reanalyses. The 1950–1976 mean precipitation and circulation from GFDL AM2.1 and NCAR CAM3 GOGAI ensemble runs are shown in Fig. 1c, d. Both models capture the broad circulation features revealed by the reanalyses. On regional scales, however, there exist systematic discrepancies among the model simulations, observations, and reanalyses. For example, the simulated 850 hPa anticyclonic winds over East China and Northwestern Pacific, which are part of the western Pacific subtropical high, are stronger than the reanalyses and the location is located to the north and west of the reanalyses. These circulation biases result in the northward shift of the rain-belt, so that the simulated precipitation is more (less) than the observation over North China (southeastern China). This is especially true for the CAM3. The results from the CAM3 and AM2.1 are consistent with Kang et al. (2002), who analyzed simulations from 10 AGCMs and found that none of the models reproduce the observed Mei-yu rain band in the region from the East China Sea to the central Pacific.

The composite differences of JJA 850 hPa winds and 200 hPa zonal wind from the NCEP/NCAR and ERA-40 reanalyses, AM2.1 GOGAI and CAM3 GOGAI ensemble runs are shown in Fig. 1e–h. The reanalyses, especially the NCEP/NCAR, clearly show that the summer monsoonal flow from Southwest China to Northeast China weakened substantially from 1950–1976 to 1977–2000, resulting in anomalous northerly winds over most East Asia and southward shift of the high-level jet. The long-term mean (1950–1976) circulation (Fig. 1a, b) reveals southwesterlies over East China that transport water vapor all the way to North China. With the anomalous northerly winds shown in Fig. 1e–h, the actual northward transport of tropical water vapor to North China has reduced while

Fig. 1 Left column: 1950–1976 mean JJA precipitation (color, mm/day), 850 hPa winds (vectors, m/s) and 200 hPa zonal wind (contours, m/s) from (**a**) observations (Chen et al. (2002)) and NCEP/NCAR reanalysis, (**b**) observations (Chen et al. (2002)) and ERA-40 reanalysis, (**c**) AM2.1 GOGAI runs, and (**d**) CAM3 GOGAI runs. Right column: the 1977–2000 minus 1950–1976 difference of JJA mean 850 hPa winds (vectors, m/s, only values that are statistically significant at the 5% level are shown) and 200 hPa zonal wind (contours, m/s, interval = 1 m/s, *dashed lines* are for negative values, *shaded areas* are statistically significant at the 5% level) from (**e**) NCEP/NCAR reanalysis, (**f**) ERA-40 reanalysis, (**g**) AM2.1 GOGAI runs, and (**h**) CAM3 GOGAI runs

more water vapor converges over the Yangtze River Valley under the weakened southerly winds during the latter period. This results in increased moisture convergence and excessive rainfall in the South and deficient rainfall in the North, as reported previously (e.g., Hu et al. 2003; Zhou and Yu 2005; Li et al. 2008). Although there exist differences between the NCEP/NCAR and ERA-40 results (e.g., smaller changes in 850 hPa winds in the ERA-40), both of them show that the 200 hPa zonal wind strengthened south of about 40°N and weakened north of about 40°N, and the 850 hPa southerlies weakened from 1950–1976 to 1977–2000. Both models capture the changes of the 200 hPa

zonal wind and 850 hPa vector winds revealed by the reanalyses over East Asia. However, the simulated 850 hPa wind changes are not as strong as those in the reanalyses and the simulated 200 hPa zonal wind changes are shifted slightly northward compared with the reanalyses. The models also produce anticyclonic wind changes over western North Pacific and cyclonic wind changes over the Bay of Bengal that are not evident in the reanalyses.

The precipitation changes from 1950–1976 to 1977–2000 from observations, AM2.1 and CAM3 GOGAI ensemble runs are shown in Fig. 2. Despite the reasonable simulation of the circulation changes over East Asia, large
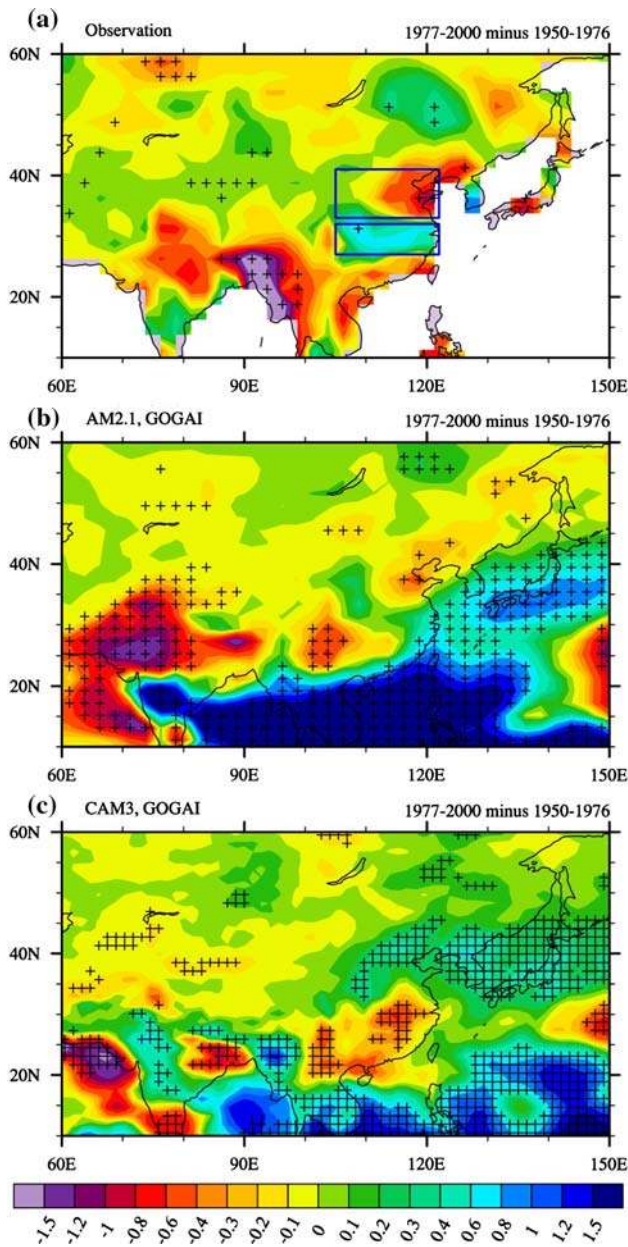
Fig. 2 The 1977–2000 minus 1950–1976 difference of JJA mean precipitation (*color*) from (**a**) observations (Chen et al. (2002)), (**b**) AM2.1 GOGAI runs, and (**c**) CAM3 GOGAI runs. The *pluses* indicate where the precipitation change is statistically significant at the 5% level. The *blue rectangular boxes* in (**a**) show the regions used for calculating the precipitation deference index (PDI), and they represent North China (33°–41°N, 105°–122°E) and the Yangtze River valley (27°–32°N, 105°–122°E)

Fig. 3 Time series of the EASMI (*bars*) and its trend line (*dashed line*) from (**a**) NCEP/NCAR reanalysis, (**b**) ERA-40 reanalysis, (**c**) AM2.1 GOGAI runs, and (**d**) CAM3 GOGAI runs. The EASMI is defined as the normalized zonal wind shear between 850 and 200 hPa averaged over 20°–40°N and 110°–140°E. Also shown are the slope of the trend (*b*, change per 50 years) and the correlation coefficient (*r*, the numbers in parentheses show the correlation of detrended series) between the EASMI shown in the panel and in (**a**)

differences exist for the precipitation change between the two models and between the observation and simulations. The precipitation change pattern over East China from the AM2.1 (Fig. 2b) roughly resembles that of the observation, whereas the CAM3-simulated changes are opposite to the observations with deficient rainfall along the Yangtze

River valley and excessive rainfall over North China. Under the SST plus greenhouse gas and aerosol forcing, both models produce more precipitation over the Tropics (south of ~20°N) and the western North Pacific Ocean, where increased SSTs enhance local convection. The models also show some drying over parts of South China and of inland East Asia just northwest of the enhanced rainband, presumably resulting from increased subsidence associated with the enhanced convection to the south and east.

Figure 3 shows the zonal wind shear-based EASMI (bars) from the NCEP/NCAR and ERA-40 reanalyses, and the AM2.1 and CAM3 GOGAI ensemble runs. The EASMI from both AM2.1 and CAM3 simulations shows decreasing trends similar to that revealed by the reanalyses, with mostly positive phases before the 1970s and negative phases in the 1980s and 1990s. The decreasing trend is steepest for the NCEP/NCAR reanalysis (−2.13/ 50 years) and they are all statistically significant at the 5%
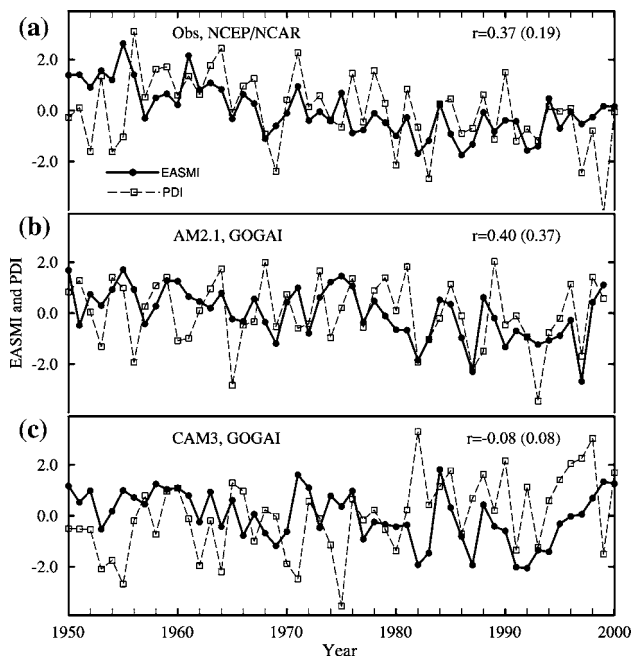
Fig. 4 Time series of the EASMI (*solid lines with dots*), the precipitation difference index (PDI, *dashed lines* with *open squares*) from (**a**) NCEP/NCAR reanalysis and Chen et al. (2002), (**b**) AM2.1 GOGAI runs, and (**c**) CAM3 GOGAI runs. The PDI is defined as the difference of the normalized precipitation between North China (33°–41°N, 105°–122°E) and the Yangtze River Valley (27°–32°N, 105°–122°E). The correlation coefficient (*r*, the numbers in parentheses show the correlation of detrended series) between the two curves is also shown

level. The EASMI time series from the two reanalyses are highly correlated (*r* = 0.97), while the model-simulated EASMI is significantly correlated with the EASMI from the NCEP/NCAR reanalysis at a moderate level (*r* = 0.64 and 0.56 for AM2.1 and CAM3, and *r* = 0. 46 and 0.47 after detrending, both are statistically significant at the 5% level).

To reveal the relationship between changes in the EASM circulation and precipitation over East China, Fig. 4 compares the time series of the EASMI (solid lines with dots) and the PDI (dash lines with open squares). The PDI from observations shows a decreasing trend (−1.78/50 years), especially from the mid-1950s to the late 1990s, which is statistically significant at the 5% level. A decreasing trend is also shown in the AM2.1 simulations (−0.69/50 years) but statistically insignificant. However, the CAM3 simulated precipitation shows a significant increasing trend (2.22/50 years) at the 5% level. Modest but statistically significant correlation between the EASMI and PDI exists in the NCEP/NCAR reanalysis EASMI and the observed PDI, but the correlation is insignificant after detrending. This correlation is reproduced in the AM2.1 simulations, but not in the CAM3. We also examined the correlation between the EASMI and PDI with 5-year

running mean. The correlation coefficients increase to 0.43, 0.62, and −0.33 comparing with the unsmoothed time series (0.37, 0.40, and −0.08), however the discrepancy simulated by CAM3 also becomes larger. The above statistical results indicate that the co-variance of EASMI and PDI time series mainly comes from linear trends and longer time scale variations. Thus the current state-of-the-art AGCMs may not be able to reasonably simulate the East Asian monsoon rainfall change as previously reported (Zhou and Li 2002; Zhou et al. 2008c).

3.2 EASM's response to SST forcing

Figure 5 shows the composite (1977–2000 minus 1950–1976) differences of JJA 850 hPa winds and 200 hPa zonal wind from the NCEP/NCAR reanalyses, AM2.1 GOGA, CAM3 GOGA, and CAM3 TOGA ensemble runs. Under the global SST forcing alone, both models capture the broad features of summer circulation changes from the reanalyses. Compared with Fig. 1g, h, the wind changes under the SST forcing are even larger than those under the SST plus greenhouse and aerosol forcing over East Asia. This implies that the weakening of the EASM circulation results from the SST forcing while the greenhouse gas plus aerosol forcing works in the opposite direction (i.e., enhances the EASM). The GOGA and TOGA simulations by the CAM3 (Fig. 5c, d) show similar circulation changes, which suggests that the tropical SST changes are the primary forcing for the observed EASM circulation changes.

The precipitation changes from observations and the model simulations forced by SSTs are shown in Fig. 6. The precipitation change pattern over East China from the AM2.1 GOGA runs (Fig. 6b) roughly resembles that of observations but is shifted northward, and the precipitation change pattern from the AM2.1 GOGAI (see Fig. 2b) is closer to observations than the AM2.1 GOGA runs. Similar to GOGAI simulations, both models show large precipitation increases over the western Pacific and Southeast Asia, where increased SSTs enhance local convection. The precipitation changes from the CAM3 GOGA and TOGA runs (Fig. 6c, d) are similar, which is consistent with the circulation result and further suggests the dominant effect of tropical SSTs on East Asian climate.

Figure 7 shows the EASMI time series from the NCEP/NCAR reanalyses and SST-forced runs. As in the GOGAI runs, significant downward trends are reproduced by both models. These trends are substantially stronger in the GOGA runs than the GOGAI cases in the CAM3, whereas the impact of the greenhouse gas plus aerosol forcing is much smaller in the AM2.1 (Fig. 7). The correlation coefficient with the NCEP/NCAR reanalysis EASMI is improved to 0.62 for CAM3 GOGA runs from 0.56 in its GOGAI runs, while it is slightly reduced in the AM2.1
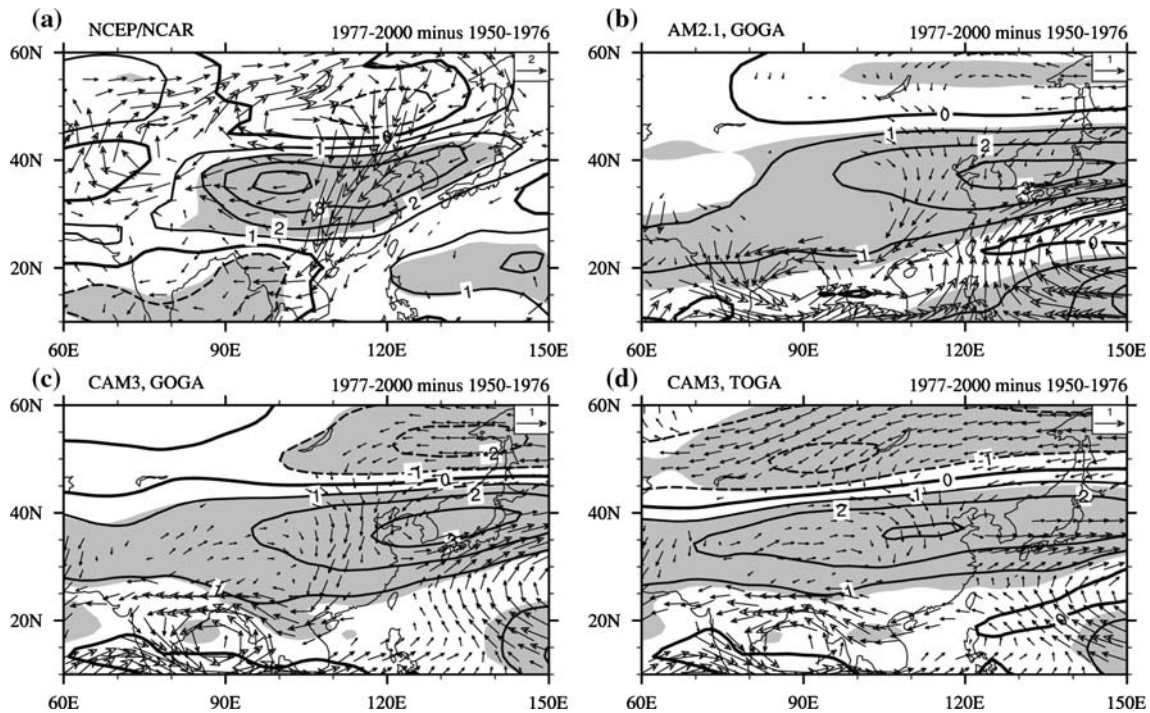
Fig. 5 The 1977–2000 minus 1950–1976 difference of JJA mean 850 hPa winds (vectors, m/s, only values that are statistically significant at the 5% level are shown) and 200 hPa zonal wind (contours, m/s, interval = 1 m/s, *dashed lines* are for negative values, *shading* indicates statistically significant at the 5% level) from (**a**) NCEP/NCAR reanalysis, (**b**) AM2.1 GOGA runs, (**c**) CAM3 GOGA runs, and (**d**) CAM3 TOGA runs. Figure 1e is repeated here in panel (**a**) for comparison
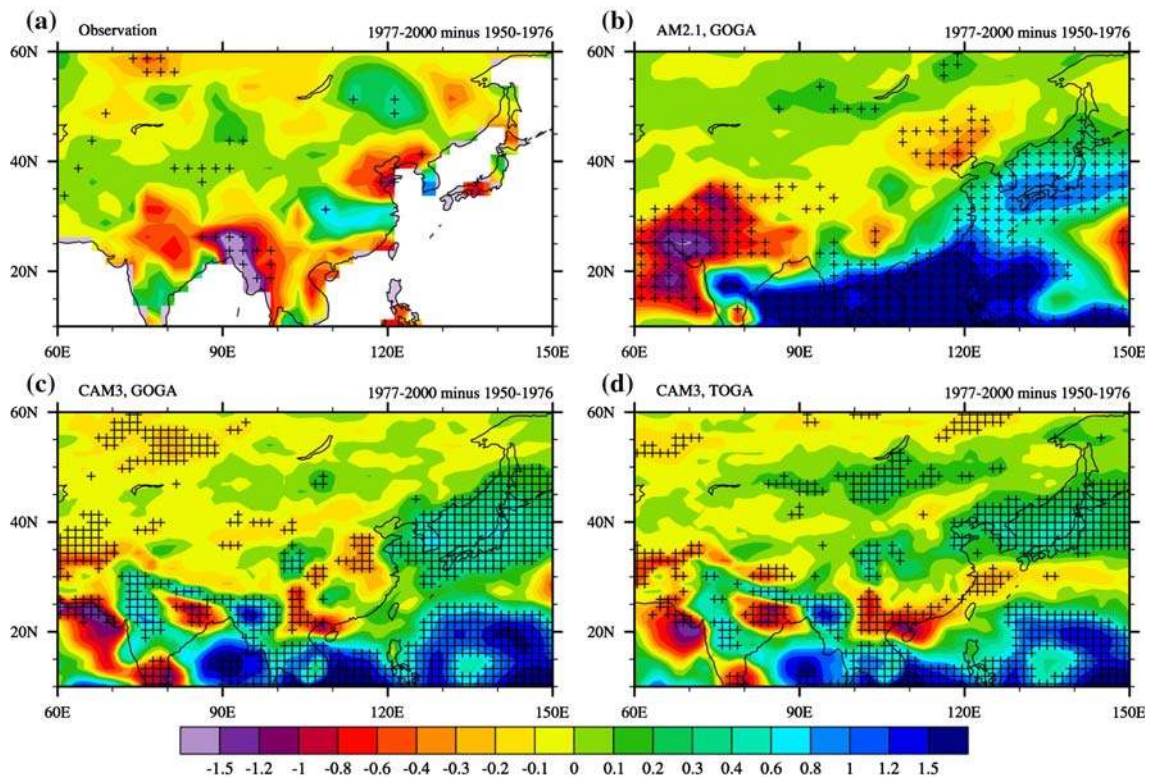

Fig. 6 The 1977–2000 minus 1950–1976 difference of JJA mean precipitation (color) from (**a**) observations, (**b**) AM2.1 GOGA runs, (**c**) CAM3 GOGA runs, and (**d**) CAM3 TOGA runs. The *pluses* indicate where the precipitation change is statistically significant at the 5% level. Figure 2a is repeated here in panel (**a**) for comparison
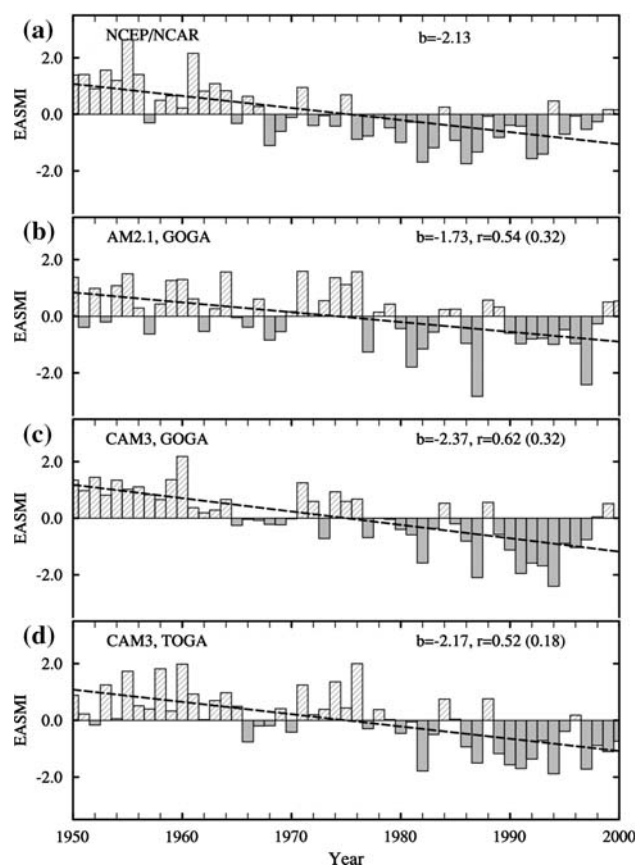
Fig. 7 Time series of the EASMI (*bars*) and its *trend line* (*dashed line*) from (**a**) NCEP/NCAR reanalysis, (**b**) AM2.1 GOGA runs, (**c**) CAM3 GOGA runs, and (**d**) CAM3 TOGA runs. Also shown are the slope of the trend (*b*, change per 50 years) and the correlation coefficient (*r*, the numbers in parentheses show the correlation of detrended series) between the EASMI shown in the panel and in (**a**). Figure 3a is repeated here in panel (**a**) for comparison

from 0.64 in the GOGAI runs to 0.54 in the GOGA runs. After detrending, the correlation between the EASMIs from the NCEP/NCAR reanalyses and the GOGA and GOGAI simulations is still statistically significant at the 5% level. However, the correlation between the EASMIs from the TOGA simulation and NCEP/NCAR reanalyses is insignificant, which indicates that the higher correlation between the un-detrended time series results mainly from the long-term trends. Similar to Fig. 4, correlations between the EASMI and PDI remain weak in the GOGA runs (not shown).

To examine the vertical structure of the changes in temperature and winds, Fig. 8 shows a cross section of the 1950–1976 mean JJA temperature (contours) and vector winds along 105°–122°E (the same longitudes for the PDI) from the NCEP/NCAR reanalyses and the AM2.1 GOGA runs (Fig. 8a, b), along with their decadal changes (Fig. 8c, d) and the changes from the CAM3 GOGA and TOGA runs (Fig. 8e, f). The NCEP/NCAR reanalyses shows relatively

warm air and corresponding upward motion over Southeast Asia (∼10°–30°N) (Fig. 8a), with weak upward motion north of ∼40°N. The AM2.1 model roughly reproduces this broad feature, with the strongest upward motion shifted southward. The changes from the reanalyses (Fig. 8c) show cooling over the land (north of ∼25°N) and warming over the ocean (south of ∼25°N) during 1977–2000 relative to 1950–1976. Accompanying this change in land-ocean temperature gradients, anomalous descending and ascending motion occurs over the northern land and southern ocean areas, respectively, with anomalous northerly winds between 20° and 50°N (Fig. 8c). The strongest cooling center is around the 300 hPa level. Yu et al. (2004) showed that this cooling center can enhance the southern part of the high level jet stream and weaken the northern part of the high level jet stream through the geostrophic balance, resulting in the southward shift of high level jet while enhancing anomalous low-level northerlies on the southeastern part of the cooling center (Xin et al. 2006). In summary, the temperature and associated circulation changes shown in Fig. 8c are consistent with a weakened EASM (i.e., weaker southerly winds over East China, cf. Fig. 1e, f).

Both the AM2.1 (Fig. 8d) and CAM3 (Fig. 8e, f) models broadly reproduce the changes in the land-sea temperature gradient and upper-level cooling over East Asian land as the EASM weakens. This result suggests that the SST changes, especially those in the Tropics, induce tropospheric warming over the tropical ocean and cooling over the extratropical land in the East Asian sector, which weakens the summer land-ocean temperature gradient and thus the EASM.

Figure 9a, b show that the CAM3 reproduces, in its GOGA (and TOGA) runs, the correlation patterns between the observed SST and the EASMI from the NCEP/NCAR reanalyses. Significant negative correlations of 0.5–0.7 are seen over the tropical central and eastern Pacific and central Indian Ocean, while positive correlations exist over the North and South Pacific. The correlation patterns shown in Fig. 9a, b resemble that of the SST mode associated with ENSO (Guan and Nigam 2008), which in turn resembles that of the tropical interdecadal climate variability (Deser et al. 2004). The negative correlation over the tropical oceans suggests that warming in both the tropical Pacific and Indian Ocean leads to weakening of the EASM.

The correlation with SSTs over the North Pacific suggests a link to the Pacific decadal oscillation (PDO), which is largely originated from the tropical interdecadal variability that centers over the tropical central and eastern Pacific Ocean (Deser et al. 2004; Deser and Phillips 2006). Indeed, the observed PDO index (bars in Fig. 9c) is significantly correlated with the EASMI based on the NCEP/NCAR reanalyses (cf. Fig. 3a; $r = -0.67$). Figure 9c

Fig. 8 Mean latitude-height cross section averaged over 105°–122°E of JJA temperature (contours, K) and meridional circulation (vectors, only values that are statistically significant at the 5% level are shown, units of the vertical and meridional velocity are -10^{-4} hPa/s and m/s, respectively) for 1950–1976 mean from (**a**) NCEP/NCAR reanalysis and (**b**) AM2.1 GOGA runs, and for 1977–2000 minus 1950–1976 difference from (**c**) NCEP/NCAR reanalysis, (**d**) AM2.1 GOGA runs, (**e**) CAM3 GOGA runs, and (**f**) CAM3 TOGA runs. The contour interval is 10 K in (**a**)-(**b**) and 0.2 K in (**c**)–(**f**) with *dashed lines* for negative values. The shaded areas in (**c**)–(**f**) are statistically significant at the 5% level
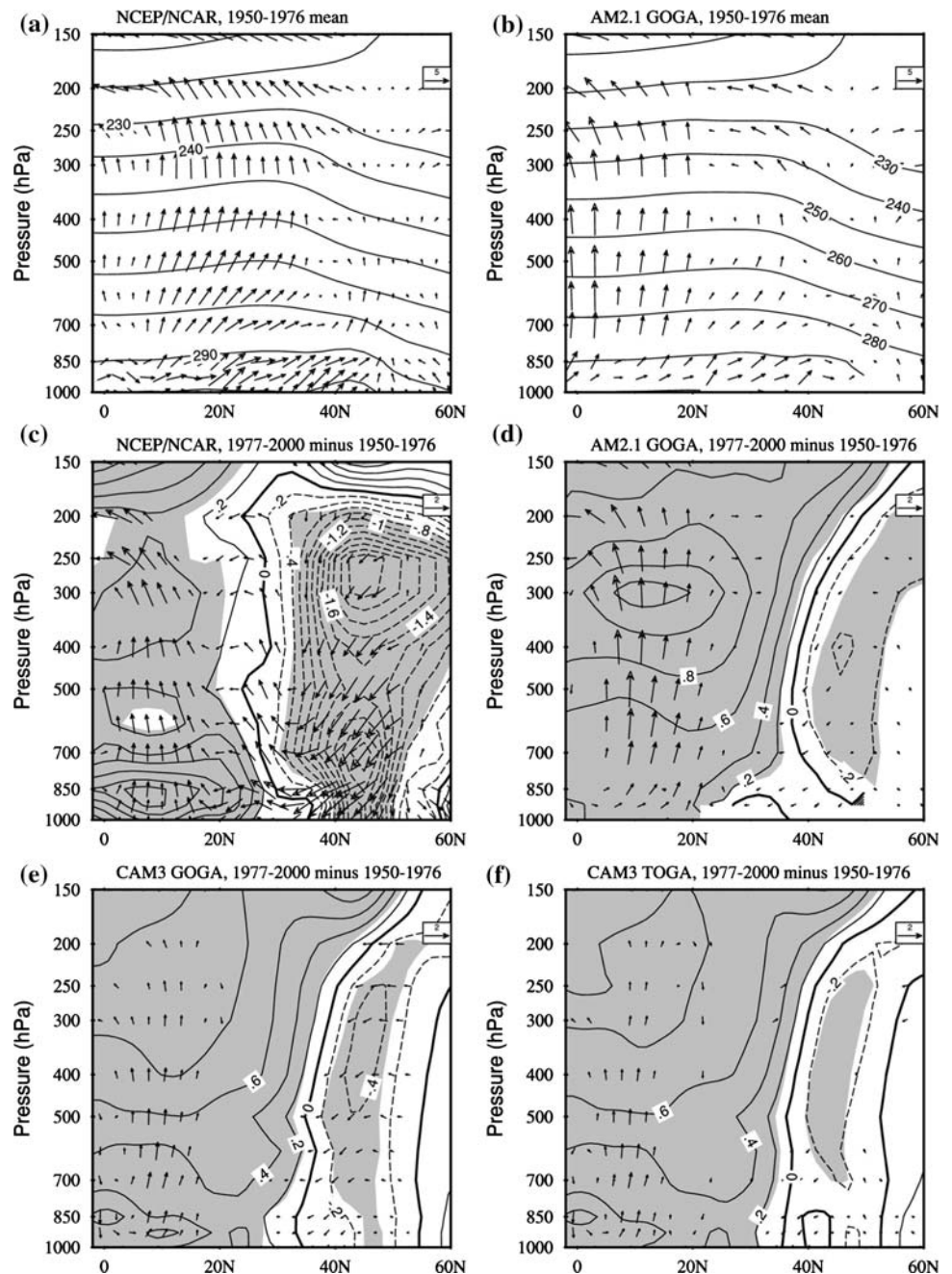
shows that the EASMI time series from the CAM3 GOGA and TOGA runs are similarly correlated with the observed PDO index, with much of the co-variance mainly comes from decadal and long-term changes. This further suggests a major effect of tropical SSTs (primarily over the central and eastern Pacific) on the EASM, and that the EASM's association with the PDO results largely from the fact that both the PDO and EASM are significantly influenced by the tropical interdecadal variability as described in Deser et al. (2004).

3.3 EASM's response to atmospheric forcings

The combined effect of the IPCC atmospheric forcings, primarily greenhouse gases and aerosols (direct effects only) is simulated by the CAM3 T42 RADATM runs, with the composite wind changes shown in Fig. 10a. We emphasize that the effect of greenhouse gas-induced warming over the oceans is largely excluded because of the fixed SSTs in these simulations, which focus on the local radiative effect of the greenhouse gases and aerosols over
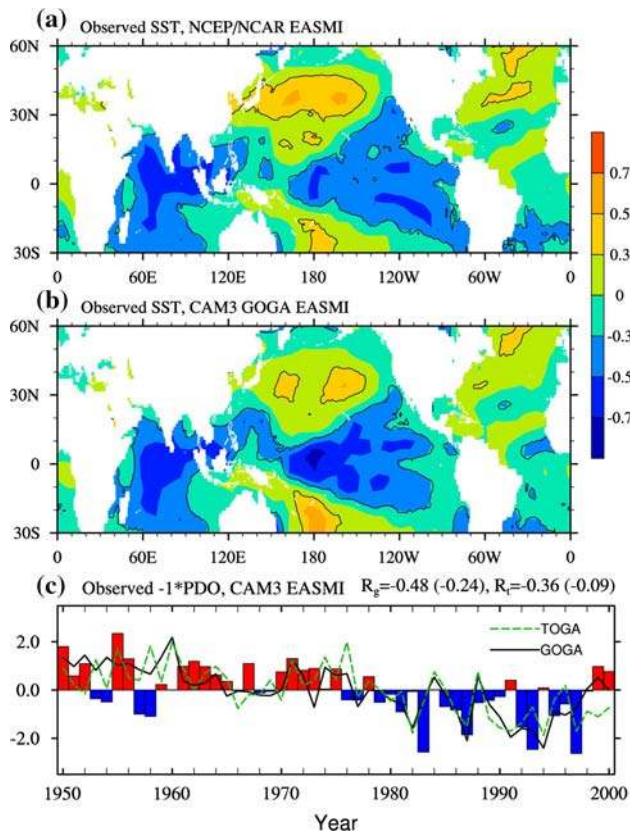
Fig. 9 Correlation coefficient between observed JJA SST at each grid box and the EASMI from (**a**) NCEP/NCAR reanalysis and (**b**) CAM3 GOGA runs. Values above the contour line are significant at the 5% level. (**c**) Time series of the observed JJA PDO index (multiplied by −1, *bars*) and the EASMI from the CAM3 GOGA (*solid black line*) and TOGA (*dashed green line*) simulations. The R_g (R_t) on top of panel (**c**) is the correlation coefficient between the observed PDO index and GOGA (TOGA) simulated EASMI, the numbers in parentheses show the correlation of detrended series

land. Figure 10a, b show that the CAM3 T42 GOGAI minus GOGA results exhibit change patterns similar to those from the CAM3 RADATM runs, which suggests that the climatic effects of the SST and atmospheric forcings are quasi-linear. Since RADATM runs for CAM3 T85 and AM2.1 are unavailable, we use the GOGAI minus GOGA result as a proxy in Fig. 10c, d. Both the CAM3 and AM2.1 show that the atmospheric forcings over land induce stronger southerly low-level winds and weaker zonal wind component around 23°–43°N over East Asia, with the high-level jet shifted northward (Fig. 10). The EASMI time series from the atmospheric forcing experiments (Fig. 11) all show upward trends, although the trend for AM2.1 GOGAI-GOGA case is small and insignificant. These changes are opposite to those from the reanalyses and SST-forced model simulations (cf. Figs. 3 and 7). The strengthening of the EASM is consistent with analyses of coupled climate model simulations by Hu et al. (2000) and Bueh et al. (2003), who showed that increased future

greenhouse gas concentrations intensify the EASM because of an enhanced land-ocean temperature gradient due to larger warming over land. In our experiments, near-surface summer temperatures over Asia increased under increasing greenhouse gases while the SSTs were fixed to climatological values, so that the land-ocean (surface) temperature gradient was enhanced, resulting in a stronger EASM.

The combined effect of the atmospheric forcings on precipitation (not shown) is roughly the opposite to that of the SST forcing (cf. Fig. 6), with decreases over most of the oceans surrounding East Asia but increases over most of the land areas in this region.

We realize that in the real world increased greenhouse gases also warm the oceans, thus the IPCC forcing runs with fixed SST do not fully account for the effects of increased greenhouse gases and other atmospheric forcings (e.g., through air-sea feedback). Nevertheless, the results from the RADATM runs still qualitatively emulate the situation in which summer land temperature increases faster than SSTs (like in projected future climates). We notice that the magnitude of the circulation changes produced by the atmospheric forcings is smaller than that by the SST forcing, and that the results from the GOGA runs (Figs. 5–7) are similar to those from the GOGAI runs (Figs. 1–3). This suggests that at least for these two models the observed SST forcing dominates over the greenhouse gas plus (direct) aerosol forcing during 1950–2000.

4 Summary and concluding remarks

4.1 Summary

East Asian climate has experienced anomalous low-level northeasterlies, southward shift of high level jets, and "southern flooding and northern drought" precipitation changes from 1950–1976 to 1977–2000. We have analyzed ensemble runs from 1950 to 2000 by two different AGCMs, namely the NCAR CAM3 and GFDL AM2.1, forced separately by observed tropical SSTs, global SSTs, atmospheric forcings (primarily greenhouse gases plus the direct effect of aerosols), and a combination of global SSTs and atmospheric forcings. The main findings are as follows.

The simulations from both models show that the observed SST forcing, primarily from the Tropics, is able to induce most of the observed circulation changes associated with the weakening of the EASM since the 1970s. The simulated EASM circulation changes from runs forced separately with global and tropical SSTs are comparable, and the simulated EASM indices have similar variations that are correlated with the observed PDO index. These results, combined with previous studies (e.g., Deser et al. 2004; Deser and Phillips 2006), suggest that the recent
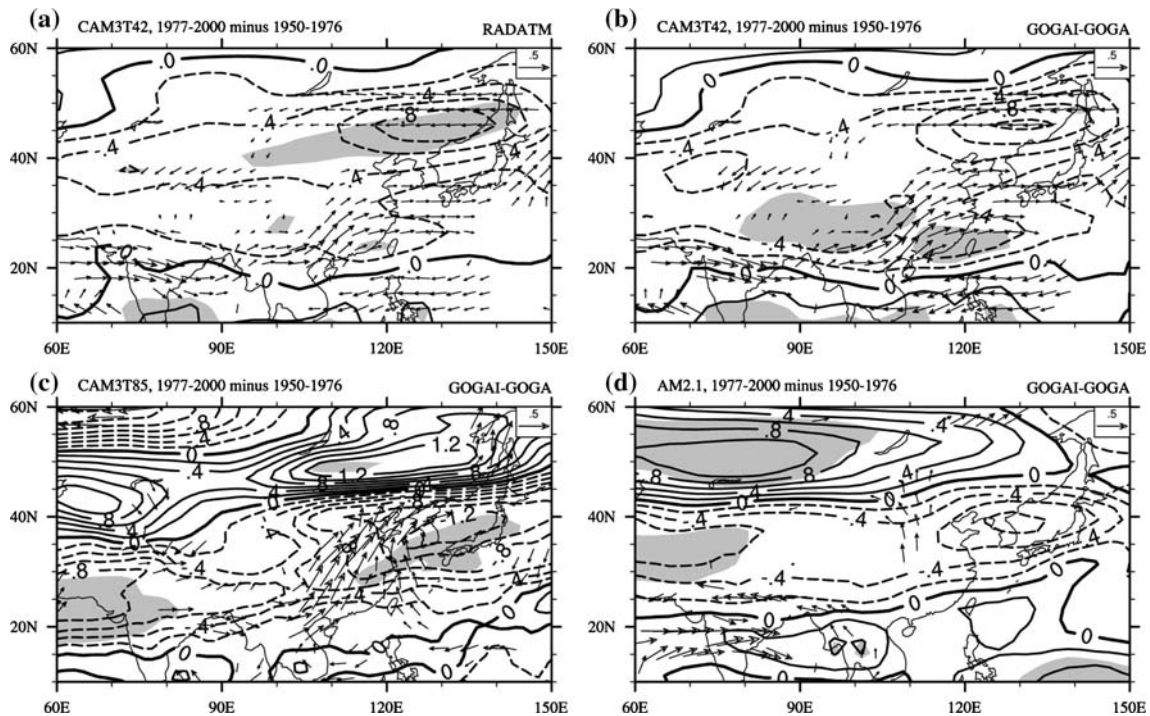
Fig. 10 The 1977–2000 minus 1950–1976 difference of JJA mean 850 hPa winds (vectors, m/s, only values that are statistically significant at the 5% level are shown) and 200 hPa zonal wind (contours, interval is 0.2 m/s, *dashed lines* for negative values, the shaded areas are statistically significant at the 5% level) from (**a**) CAM3 T42 RADATM runs, (**b**) CAM3 T42 GOGAI minus GOGA runs, (**c**) CAM3 T85 GOGAI minus GOGA runs, and (**d**) AM2.1 GOGAI minus GOGA runs

warming over tropical oceans, especially those associated with the tropical interdecadal variability centered over the central and eastern Pacific, has played a major role in the weakening of the EASM during recent decades.

The atmospheric forcings (primarily greenhouse gases plus the direct effect of aerosols) during 1950–2000 increase the summer land-ocean temperature contrast and thus enhance the EASM. This is opposite to the NCEP/NCAR and ERA-40 reanalyses and the SST-forced simulations, although the changes are smaller than those under the SST forcing.

Results from runs forced by both the SST and atmospheric forcing are comparable to those from runs forced by the SST forcing alone. This indicates that the observed SST forcing dominates over the atmospheric forcing during 1950–2000 for East Asian climate.

4.2 Discussion

The SST-forcing produces increased summer precipitation over the northern Indian Ocean and the western Pacific Ocean but drying over the land areas northwest of these oceanic areas, whereas the atmospheric forcing produces roughly the opposite precipitation change patterns. Despite the reasonable simulations of the observed circulation changes, the two global models failed to reproduce the relatively small-scale rainfall change patterns over East China during recent decades. The rain-belt associated with the EASM is a regional feature associated with the monsoon front. A realistic simulation of this rain-belt and its decadal change still remains a challenge for current global models. Wang et al. (2005) have shown that air-sea interactions are crucial for the simulation of SST-rainfall relationships over monsoon regions where atmospheric feedback on SST is critical. Using AGCMs, instead of coupled atmosphere-ocean models, may not adequately represent the air-sea interactions, which could contribute to the deficiencies in rainfall simulations over East China. Moreover, the relatively low model resolution can not resolve the complex terrain over Asia, which could also lead to errors in simulating the monsoon rainfall. Finally, the versions of the CAM3 and AM2.1 used here only include the direct effect and do not consider indirect effects of aerosols. This could underestimate the actual effects of anthropogenic aerosols on the EASM.

The classical view is that the northward water vapor transport can only reach the Yangtze River Valley as the EASM weakens, which leads to increased moisture convergence and thus frequent flooding in the Yangtze River Valley but drying in North China. From this perspective, our model results suggest that recent warming in the Tropics, especially the warming associated with the tropical
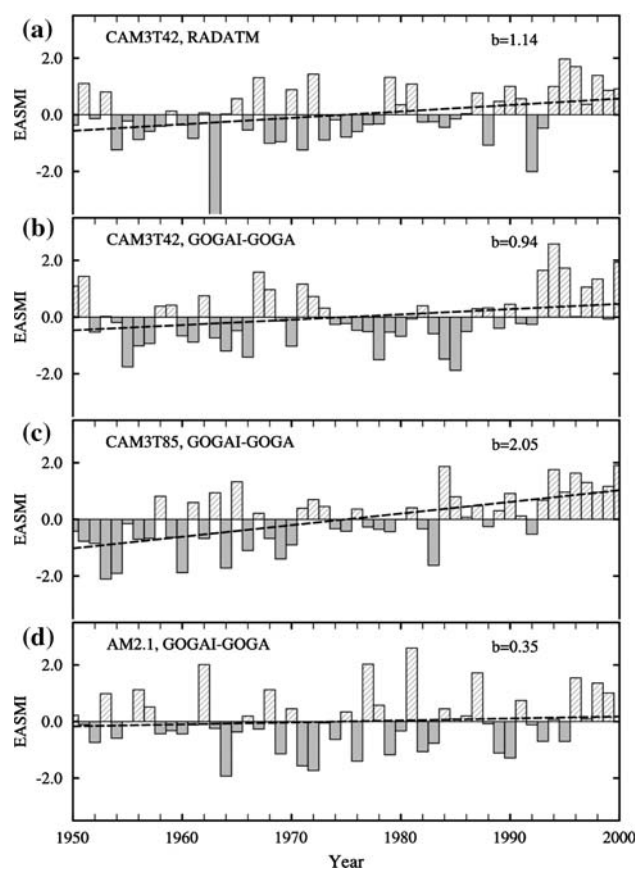
Fig. 11 Time series of the EASMI (*bars*) and its *trend line* (*dashed line*, *b* is the slope in changes per 50 years) from (**a**) CAM3 T42 RADATM runs, (**b**) CAM3 T42 GOGAI minus GOGA runs, (**c**) CAM3 T85 GOGAI minus GOGA runs, and (**d**) AM2.1 GOGAI minus GOGA runs

interdecadal variability centered over the central and eastern Pacific, is a major cause for the weakening of the EASM and the associated rainfall changes over East Asia since the 1970s. This tropical interdecadal variability influences SSTs and other climate fields in the Indian Ocean, the North and South Pacific Ocean via the mechanism of atmospheric bridge (Deser et al. 2004). Therefore, it is likely that the EASM's association with SST variability and changes in the Indian and North Pacific Ocean found in previous studies (see Sect. 1) may all be linked to the same tropical interdecadal variability originated from the central and eastern Pacific Ocean.

In addition, the EASM index used in our discussion represents a measure of strength of large-scale forcing linked to tropical convective activity (Wang et al. 1999). It is better than the conventionally used sea level pressure (SLP) difference index across East Asia and North Pacific such as Guo et al. (2003) in describing the monsoon-tropical Pacific connections. Specifying SST to an AGCM generally shows poor performance in reproducing the SLP response over the North Pacific and the associated changes

of SLP difference index (Zhou et al. 2008d). This deficiency is also seen in our model results as evidenced by the spurious anticyclone over the North Pacific (cf. Fig. 1e–h).

References

Bueh C, Cubasch U, Hagemann S (2003) Impacts of global warming on changes in the East Asian monsoon and the related river discharge in a global time-slice experiment. Clim Res 24:47–57. doi:10.3354/cr024047

Chang C, Zhang Y, Li T (2000) Interannual and interdecadal variations of the East Asian summer monsoon and tropical Pacific SSTs. Part I: roles of the subtropical ridge. J Clim 13:4310–4325. doi:10.1175/1520-0442(2000)013<4310:IAIVOT>2.0.CO;2

Chen M, Xie P, Janowiak J, Arkin P (2002) Global land precipitation: a 50-year monthly analysis based on gauge observations. J Hydrometeorol 3:249–266. doi:10.1175/1525-7541(2002)003<0249:GLPAYM>2.0.CO;2

Collins W et al (2006) The formulation and atmospheric simulation of the community atmosphere model version 3 (CAM3). J Clim 19:2144–2161. doi:10.1175/JCLI3760.1

Dai A, Wigley T, Boville B, Kiehl J, Buja L (2001) Climates of the twentieth and twenty-first centuries simulated by the NCAR climate system model. J Clim 14:485–519. doi:10.1175/1520-0442(2001)014<0485:COTTAT>2.0.CO;2

Deser C, Phillips A, Hurrell J (2004) Pacific interdecadal climate variability: linkages between the tropics and the North Pacific during boreal winter since 1900. J Clim 17:3109–3124. doi:10.1175/1520-0442(2004)017<3109:PICVLB>2.0.CO;2

Deser C, Phillips A (2006) Simulation of the 1976/77 climate transition over the North Pacific: sensitivity to tropical forcing. J Clim 19:6170–6180. doi:10.1175/JCLI3963.1

GFDL Global Atmospheric Model Development Team (2004) The new GFDL global atmosphere and land model AM2-LM2: evaluation with prescribed SST simulations. J Clim 17:4641–4673. doi:10.1175/JCLI-3223.1

Gong D, Ho C (2002) Shift in the summer rainfall over the Yangtze River valley in the late 1970s. Geophys Res Lett 29(10):1436. doi:10.1029/2001GL014523

Guan B, Nigam S (2008) Pacific sea surface temperatures in the twentieth century: an evolution-centric analysis of variability and trend. J Clim 21:2790–2809. doi:10.1175/2007JCLI2076.1

Guo Q, Cai J, Shao X, Sha W (2003) Interdecadal variability of East-Asian summer monsoon and its impact on the climate of China. Acta Geogr Sin 58:569–576 in Chinese

Han J, Wang H (2007) Interdecadal variability of the East Asian summer monsoon in an AGCM. Adv Atmos Sci 24:808–818. doi:10.1007/s00376-007-0808-0

Hu Z (1997) Interdecadal variability of summer climate over East Asia and its association with 500 hPa height and global sea surface temperature. J Geophys Res 102(D16):19403–19412. doi:10.1029/97JD01052

Hu Z, Latif M, Roeckner E, Bengtsson L (2000) Intensified Asian summer monsoon and its variability in a coupled model forced

by increasing greenhouse gas concentrations. Geophys Res Lett 27(17):2681–2684. doi:10.1029/2000GL011550

Hu Z, Yang S, Wu R (2003) Long-term climate variations in China and global warming signals. J Geophys Res 108(D19):4614. doi:10.1029/2003JD003651

Huang Y, Dickinson R, Chameides W (2006) Impact of aerosol indirect effect on surface temperature over East Asia. Proc Natl Acad Sci USA 103(12):4371–4376. doi:10.1073/pnas.0504428103

Hurrell J, Hack J, Shea D, Caron J, Rosinski J (2008) A new sea surface temperature and sea ice boundary data set for the Community Atmosphere Model. J Clim 21(19):5145–5153. doi:10.1175/2008JCLI2292.1

Kalnay E et al (1996) The NCEP/NCAR 40-year reanalysis project. Bull Am Meteorol Soc 77:437–471. doi:10.1175/1520-0477(1996)077<0437:TNYRP>2.0.CO;2

Kang I, Jin K, Wang B, Lau K, Shukla J, Krishnamurthy V, Schubert S, Wailser D, Stern W, Kitoh A, Meehl G, Kanamitsu M, Galin V, Satyan V, Park C, Liu Y (2002) Intercomparison of the climatological variations of Asian summer monsoon precipitation simulated by 10 GCMs. Clim Dyn 19:383–395. doi:10.1007/s00382-002-0245-9

Lau K, Weng H (2001) Coherent modes of global SST and summer rainfall over China: an assessment of the regional impacts of the 1997 98 El Niño. J Clim 14:1294–1308. doi:10.1175/1520-0442(2001)014<1294:CMOGSA>2.0.CO;2

Li J, Yu R, Zhou T, Wang B (2005) Why is there an early spring cooling shift downstream of the Tibetan Plateau. J Clim 18(22):4660–4668. doi:10.1175/JCLI3568.1

Li H, Zhou T, Yu R (2008) Analysis of July–August daily precipitation characteristics variation in Eastern China during 1958–2000. Chin J Atmos Sci 32:358–371 in Chinese

Ma Z, Fu C (2007) Evidences of drying trend in the global during the later half of 20th century and their relationship with large-scale climate background. Sci China D 37:222–233 in Chinese

Menon S, Hansen J, Nazarenko L, Luo Y (2002) Climate effects of black carbon aerosols in China and India. Science 297:2250–2253. doi:10.1126/science.1075159

Nitta T, Hu Z (1996) Summer climate variability in China and its association with 500 hPa height and tropical convection. J Metab Soc Jpn 74:425–445

Qian Y, Giorgi F (1999) Interactive coupling of regional climate and sulfate aerosol models over eastern Asia. J Geophys Res 104(D6):6477–6499. doi:10.1029/98JD02347

Qian Y, Leung L, Ghan S, Giorgi F (2003) Regional climate effects of aerosols over China: modeling and observation. Tellus B Chem Phys Meteorol 55:914–934. doi:10.1046/j.1435-6935.2003.00070.x

Trenberth K, Hurrell J (1994) Decadal atmosphere-ocean variations in the Pacific. Clim Dyn 9:303–319. doi:10.1007/BF00204745

Uppala S et al (2005) The ERA-40 re-analysis. QJR Metab Soc 131:2961–3012. doi:10.1256/qj.04.176

Wang H (2001) The weakening of Asian monsoon circulation after the end of 1970s. Adv Atmos Sci 18:376–386. doi:10.1007/BF02919316

Wang B, Ding Q (2006) Changes in global monsoon precipitation over the past 56 years. Geophys Res Lett 33:L06711. doi:10.1029/2005GL025347

Wang B, Fan Z (1999) Choice of south Asian summer monsoon indices. Bull Am Meteorol Soc 80:629–638. doi:10.1175/1520-0477(1999)080<0629:COSASM>2.0.CO;2

Wang B, Wu R, Fu X (2000) Pacific-East Asian teleconnection: how does ENSO affect East Asian climate? J Clim 13:1517–1536. doi:10.1175/1520-0442(2000)013<1517:PEATHD>2.0.CO;2

Wang B, Ding Q, Fu X, Kang I, Jin K, Shukla J, Doblas-Reyes F (2005) Fundamental challenges in simulation and prediction of

summer monsoon rainfall. Geophys Res Lett 32:L15711. doi:10.1029/2005GL022734

Webster P, Yang S (1992) Monsoon and ENSO: selectively interactive systems. QJR Metab Soc 118:877–926. doi:10.1002/qj.49711850705

Weng H, Lau K, Xue Y (1999) Multi-scale summer rainfall variability over China and its long-term link to global sea surface temperature variability. J Metab Soc Jpn 77:845–857

Wu R, Wang B (2002) A contrast of the East Asian summer monsoon-ENSO relationship between 1962–77 and 1978–93. J Clim 15:3266–3279. doi:10.1175/1520-0442(2002)015<3266:ACOTEA>2.0.CO;2

Wu R, Hu Z, Kirtman B (2003) Evolution of ENSO-related rainfall anomalies in East Asia. J Clim 16(22):3742–3758. doi:10.1175/1520-0442(2003)016<3742:EOERAI>2.0.CO;2

Xin X, Yu R, Zhou T, Wang B (2006) Drought in late spring of South China in recent decades. J Clim 19(13):3197–3206. doi:10.1175/JCLI3794.1

Xu M, Chang C, Fu C, Qi Y, Robock A, Robinson D, Zhang H (2006) Steady decline of East Asian monsoon winds, 1969–2000: evidence from direct ground measurements of wind speed. J Geophys Res 111:D24111. doi:10.1029/2006JD007337

Xu Q (2001) Abrupt change of the mid-summer climate in central east China by the influence of atmospheric pollution. Atmos Environ 35:5029–5040. doi:10.1016/S1352-2310(01)00315-6

Yang F, Lau K (2004) Trend and variability of China precipitation in spring and summer: linkage to sea-surface temperatures. Int J Climatol 24:1625–1644. doi:10.1002/joc.1094

Yang X, Xie Q, Zhu Y, Sun X, Guo Y (2005) Decadal-to-interdecadal variability of precipitation in North China and associated atmospheric and oceanic anomaly patterns. Chin J Geophys 48:789–797 in Chinese

Yatagai A, Yasunari T (1994) Trends and decadal-scale fluctuations of surface air temperature and precipitation over China and Mongolia during the recent 40 year period (1951–1990). J Metab Soc Jpn 72:937–957

Yu R, Zhou T (2004) Impacts of winter NAO on March cooling trends over subtropical Eurasia continent in the recent half century. Geophys Res Lett 31:L12204. doi:10.1029/2004GL019814

Yu R, Wang B, Zhou T (2004) Tropospheric cooling and summer monsoon weakening trend over East Asia. Geophys Res Lett 31:L22212. doi:10.1029/2004GL021270

Yu R, Zhou T (2007) Seasonality and three-dimensional structure of the interdecadal change in East Asian monsoon. J Clim 20:5344–5355. doi:10.1175/2007JCLI1559.1

Zeng G, Sun Z, Wang W, Lin Z, Ni D (2007) Interdecadal variation of East Asian summer monsoon simulated by NCAR CAM3 driven by global SSTs. Clim Environ Res 12:211–224 in Chinese

Zhang Y, Wallace J, Battisti D (1997) ENSO-like interdecadal variability: 1900–93. J Clim 10:1004–1020. doi:10.1175/1520-0442(1997)010<1004:ELIV>2.0.CO;2

Zhang Y, Kuang X, Guo W, Zhou T (2006) Seasonal evolution of the upper-tropospheric westerly jet core over East Asia. Geophys Res Lett 33:L11708. doi:10.1029/2006GL026377

Zhou L, Huang R (2003) Research on the characteristics of interdecadal variability of summer climate in China and its possible cause. Clim Environ Res 8:274–290 in Chinese

Zhou T, Li Z (2002) Simulation of the East Asian summer monsoon by using a variable resolution atmospheric GCM. Clim Dyn 19:167–180. doi:10.1007/s00382-001-0214-8

Zhou T, Yu R (2005) Atmospheric water vapor transport associated with typical anomalous summer rainfall patterns in China. J Geophys Res 110:D08104. doi:10.1029/2004JD005413

Zhou T, Yu R, Zhang J, Drange H, Cassou C, Deser C, Hodson D, Sanchez-Gomez E, Li J, Keenlyside N, Xin X, Okumura Y

(2008a) Why the Western Pacific subtropical high has extended westward since the late 1970s. J Clim, in revision

Zhou T, Zhang L, Li H (2008b) Changes in global land monsoon area and total rainfall accumulation over the last half century. Geophys Res Lett 35:L16707. doi:10.1029/2008GL034881

Zhou T, Yu R, Li H, Wang B (2008c) Ocean forcing to changes in global monsoon precipitation over the recent half century. J Clim 21:3833–3852. doi:10.1175/2008JCLI2067.1

Zhou T, Wu B, Scaife AA, Brönnimann S et al (2008d) The CLIVAR C20C project: which components of the Asian–Australian monsoon circulation variations are forced and reproducible? Clim Dyn (in Revision)